Journal of ELECTRONIC MATERIALS, Vol. 48, No. 10, 2019
https://doi.org/10.1007/s11664-019-07362-9

Optical Properties of MBE-Grown $Hg_{1-x}Cd_xSe$

W.W. PAN,[1] Z.K. ZHANG,[1] W. LEI,[1,2] and L. FARAONE[1]

1.—Department of Electrical Electronic and Computer Engineering, The University of Western Australia, 35 Stirling Highway, Crawley, WA 6009, Australia. 2.—e-mail: wen.lei@uwa.edu.au

In this work, we present a study on the temperature-dependent infrared absorption spectra of $Hg_{1-x}Cd_xSe$ grown by molecular beam epitaxy (MBE) on GaSb (211) substrate, having a nominal x-value of 0.21. For temperatures below 200 K, the observed optical bandgap is found to correspond to the Fermi energy level rather than the intrinsic bandgap, which is quantitatively explained by the Burstein–Moss shift due to the presence of a background electron concentration of 3.5×10^{16} cm^{-3}. In addition, empirical formulae for calculating both the absorption edge and intrinsic absorption coefficient in the Kane region have been derived from the previously reported absorption spectra of Bridgeman-grown $Hg_{1-x}Cd_xSe$ samples ($0.15 \le x \le 0.3$). By employing the empirical expressions, the infrared transmission spectra have been modeled based on the characteristic matrix method, and the x value profile of the sample along the growth direction has been determined, which is in good agreement with the experimental results obtained from secondary ion mass spectrometry (SIMS) depth profiling combined with Rutherford backscattering spectrometry (RBS).

Key words: HgCdSe, FTIR, transmission, absorption

INTRODUCTION

Recently, mercury cadmium selenide ($Hg_{1-x}Cd_xSe$, MCS) alloys have attracted considerable interest due to their potential application as an alternative material for next generation infrared (IR) detectors.[1–5] Current high-performance IR technology is based on mercury cadmium telluride (HgCdTe) grown on lattice-matched CdZnTe substrates which, however, suffer from severe limitations, including high cost and limited wafer size.[6–8] To address these issues, large-area Si, Ge and GaAs substrates have been proposed as replacements for CdZnTe substrates.[9–13] However, due to the large lattice-mismatch between HgCdTe and these substrates, none of them yields HgCdTe with material quality and detector performance comparable to those grown on CdZnTe. More recently, GaSb, as an alternative large area and cost effective substrate in comparison to CdZnTe, has also been proposed as a suitable substrate to replace CdZnTe for growing high-quality HgCdTe materials,[14–16] but significant further effort is needed before it can be applied in industry.

As a family member of the II–VI semiconductor alloys, $Hg_{1-x}Cd_xSe$ is crystallized in a cubic zinc-blende structure consisting of semimetal mercury selluride (HgSe) and semiconductor cadmium selenide (CdSe).[17,18] Similar to $Hg_{1-x}Cd_xTe$ in terms of IR capability, the electronic bandgap of $Hg_{1-x}Cd_xSe$ can be tuned from short-wave infrared (SWIR) to very long-wave infrared (VLWIR) by simply adjusting its alloy composition (x-value).[5] More importantly, HgCdSe is nearly lattice-matched to GaSb. Therefore, it has been considered promising as a candidate for the development of GaSb-based HgCdSe IR detectors with features of larger array format size and lower production cost.[19,20] Although some work has been undertaken on the molecular beam epitaxy (MBE) growth of HgCdSe materials,[1,2,4,9,19–25] significant further effort is needed to fully understand their optical and electronic properties before realizing their ultimate application in IR detectors.

(Received November 27, 2018; accepted June 7, 2019; published online June 25, 2019)

Growing IR materials with the designed x-value and thickness is vital for achieving maximal device performance. This is especially true for both $Hg_{1-x}Cd_xTe$ and $Hg_{1-x}Cd_xSe$ since the cut off wavelength varies significantly with small changes in x value in the LWIR region ($x \sim 0.2$).[5,26] Historically, Fourier-transform infrared spectroscopy (FTIR) transmission spectra have been widely used as a fast and non-destructive method to study the optical and structural properties of both wide and narrow bandgap semiconductors, including bandgap energy, x-value, film thickness, etc. However, the Burstein–Moss (BM) effect needs to be considered[27,28] in narrow bandgap semiconductors like HgCdTe and HgCdSe,[5,29] since it may cause gross errors when determining energy gaps from FTIR transmission measurements. In addition, it has been demonstrated that the x-value and thickness of each absorption layer can be extracted accurately by modeling the transmission spectrum in a two-color HgCdTe detector structure based on the characteristic matrix method.[30] However, the premise behind this optical modeling is that the absorption coefficient of $Hg_{1-x}Cd_xTe$ has been well-established,[30,31] which is not the case for HgCdSe. The absorption coefficient is a key physical property of IR material since it determines the layer thickness in which most of the light at a given wavelength is absorbed, and thereby directly affects the quantum efficiency of IR detectors. Although the intrinsic absorption spectrum resulting from band to band transitions can be calculated theoretically based on the method described in Ref. 32, it is difficult to apply in practice. To avoid the complex quantum mechanical calculations, Chu et al.[31] have formulated empirical expressions for the absorption coefficient of HgCdTe by fitting their experimental absorption spectra. The empirical expressions not only can be used to evaluate the absorption coefficient below and above the bandgap energy (E_g), but also are very useful for material characterization and device design.[33,34]

At the University of Western Australia, MBE growth of high quality $Hg_{1-x}Cd_xSe$ thin films on GaSb (211) substrates has been reported recently.[22,23] The as-grown $Hg_{1-x}Cd_xSe$ samples show typical n-type behavior with an electron mobility in the 10^5 cm^2 V^{-1} S^{-1} range and a background electron concentration in the 10^{16} cm^{-3} range, which meet the basic material quality requirements for fabricating high-performance infrared detectors. However, for ultimate device application their physical properties need to be understood and studied further, including the optical absorption spectra. In this paper, we present a detailed description of the optical properties of MBE-grown HgCdSe IR materials on GaSb (211)B substrates. The Burstein–Moss effect was observed in the temperature-dependent IR transmission spectra of $Hg_{1-x}Cd_xSe$ with a narrow bandgap (x = 0.21). Furthermore, empirical formulae for calculating the absorption coefficient of HgCdSe were derived, and used to evaluate the compositional uniformity of the grown HgCdSe thin films.

EXPERIMENTAL DETAILS

HgCdSe thin films with a thickness of 8.7 μm and a nominal x-value of 0.21 were grown on GaSb (211) substrates using established MBE techniques, with the growth details reported in previous work.[23] The alloy composition (x-value) of $Hg_{1-x}Cd_xSe$ epitaxial layers was analyzed via Rutherford backscattering spectrometry (RBS), and the composition profile along the growth direction was obtained by secondary ion mass spectrometry (SIMS) depth profiling combined with RBS, which were undertaken at EAG Laboratories. Hall measurements combined with quantitative mobility spectrum analysis

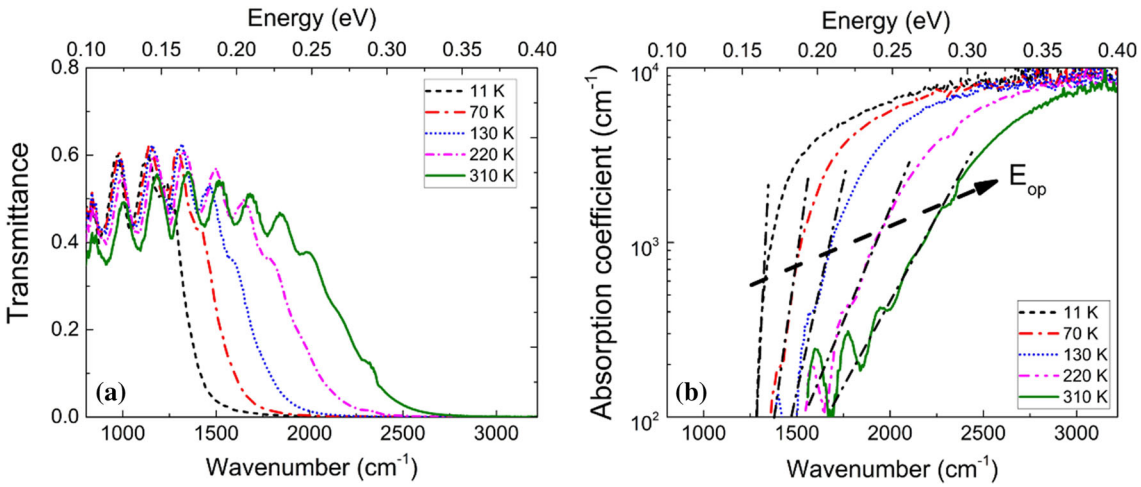

Fig. 1. (a) Representative temperature-dependent infrared transmission spectra, and (b) corresponding extracted absorption spectra, of a MBE-grown $Hg_{0.79}Cd_{0.21}Se$ thin film on GaSb (211)B substrate.

(QMSA) were performed to characterize the carrier density/concentration in the HgCdSe epitaxial layer. FTIR transmission spectra were acquired at temperatures from 11 to 310 K with a Bruker V70 FTIR spectrometer.

RESULTS AND DISCUSSION

In our FTIR measurements, the measured average transmittance of the passband for HgCdSe thin film on GaSb, labeled as $t_{\text{calculated}}$, was found to be smaller than that of a single HgCdSe layer as reported in Ref. 5, indicating the free carrier absorption in the Te-doped GaSb substrate was not insignificant. In order to eliminate this effect, we calibrated the measured transmission spectra (T_{measured}) using the following relationship:

$$\tilde{T} = \frac{t_{\text{calculated}}}{t_{\text{measured}}} T_{\text{measured}}, \tag{1}$$

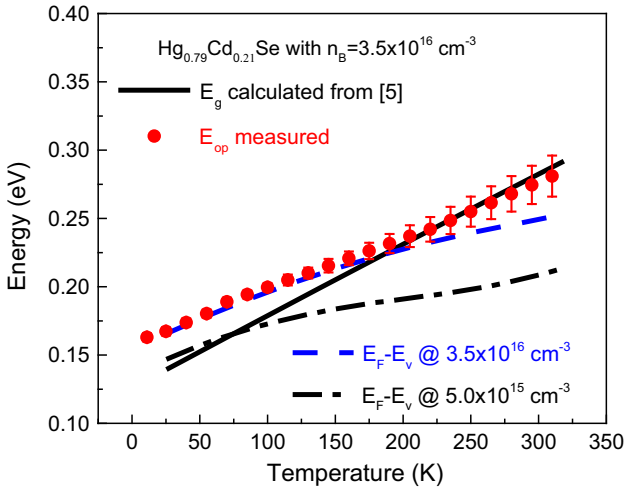

Fig. 2. Temperature dependence of the measured optical bandgap of $Hg_{0.79}Cd_{0.21}Se$ compared to calculations based on,[5] and the calculated Fermi levels for two different electron concentrations.

where $t_{\text{calculated}}$ represents the theoretical average transmittance of the passband for HgCdSe/GaSb substrate system where GaSb are considered to be transparent for the IR region studied in this work. Figure 1a shows the calibrated temperature-dependent infrared transmission spectra ($\tilde{T}$) of the MBE-grown $Hg_{0.79}Cd_{0.21}Se$ thin film. As evident from the figure, the transmission edge moves to higher energy with increasing temperature, indicating that the bandgap is positively related to the temperature increase. Moreover, at higher temperatures the transmission edge is broadened by electron–phonon interactions as well as the thermal distribution of conduction electrons due to thermal excitations. In addition, optical interference fringes are observed in the passband of the transmission spectra, and tend to extend to the transmission edge at higher temperatures. These transmission spectra were used to calculate the absorption spectra of the HgCdSe sample based on the following expressions:[5]

$$\tilde{T} = \frac{(1-R)^2 e^{-\alpha d}}{1-R^2 e^{-2\alpha d}}, \tag{2}$$

$$R = \frac{(1-n)^2}{(1+n)^2}, \tag{3}$$

where $\tilde{T}$, d, and R are the transmittance, thickness, and reflection loss of the HgCdSe layer, respectively. The refractive index of $Hg_{1-x}Cd_xSe$, n, which is a function of x value and temperature T, can be found in the open literature.[5,35] Note that the Eqs. 2 and 3 might be only valid for the air/HgCdSe/air system. However, given the refractive index of $Hg_{0.79}Cd_{0.21}Se$ we studied is varied from 3.7 to 3.3 for temperatures varying from 10 K to 310 K, and these values are quite close to that of GaSb, i.e., 3.7, the reflection loss between HgCdSe and GaSb is expected to be negligible ($< 0.6\%$) while that of both

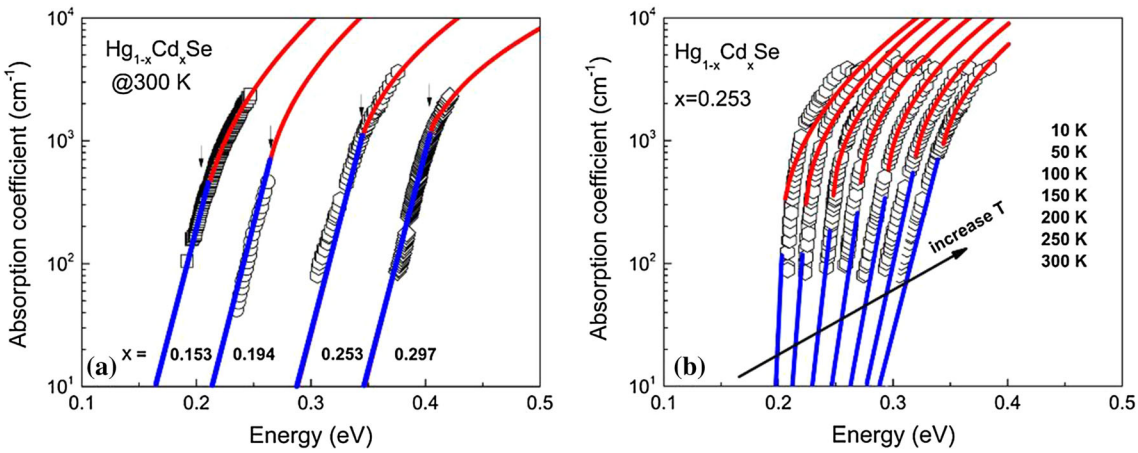

Fig. 3. (a) Composition dependent absorption coefficient of Bridgman-grown $Hg_{1-x}Cd_xSe$ at 300 K. (b) Temperature dependent absorption coefficient of Bridgman-grown $Hg_{0.747}Cd_{0.253}Te$. The dots are the experimental data obtained from Ref.[5] and the solid lines are the calculated absorption spectra of $Hg_{1-x}Cd_xSe$ from Eqs. 4 and 5 for the intrinsic region and the absorption edge, respectively.

HgCdSe/air and GaSb/air are calculated to be around 31%, suggesting the calibrated transmission spectra for HgCdSe on GaSb can be taken as the same as for a single HgCdSe layer system. The extracted absorption spectra are plotted on a log scale and displayed in Fig. 1b. As evident in Fig. 1b, each absorption spectrum is composed of two regions, namely the linear-like Urbach absorption edge[35] and the square-root-like intrinsic region.[31] The turning point between these two regions is commonly defined as the optical bandgap E_{op}, which is usually close to the value of E_g. Thus, E_{op} can be determined from the absorption spectra, although its uncertainty increases with increasing temperature due to the presence of optical interference in the transmission edge. Figure 2 shows the relationship between the E_{op} determined from the absorption spectra and temperature, indicating that the observed E_{op} increases almost linearly with increasing temperature. However, for temperatures below 200 K, the optical bandgap E_{op} deviates from the fundamental bandgap E_g, which has been calculated from the well-known empirical equation developed by Summers and Broerman.[5] The calculated E_g increases by more than 200%, from 0.131 eV to 0.283 eV when the temperature increases from 11 K to 300 K, corresponding to a temperature coefficient of 0.53 meV/K, which is significantly larger than that of the observed E_{op} which can be extrapolated to be 0.41 meV/K.

It should be noted that the as-grown HgCdSe materials typically demonstrate n-type behavior with a background electron doping concentration, n_B, in the range from low-10^{16} cm^{-3} to high-10^{18} cm^{-3}, which is believed to be caused by intrinsic Se vacancies and impurities in the materials.[1,18] For the MBE-grown HgCdSe samples in this work, the n_B was measured to be about 3.5×10^{16} cm^{-3} at 77 K.[21,22] Thus, conduction band degeneracy is expected at low temperatures for this level of electron concentration, with the Fermi level (E_F) in the conduction band and the electron states between E_F and E_C (conduction band edge) being occupied and, therefore, not contributing to optical absorption. As a result, the intrinsic absorption edge shifts to higher energies, and the resultant E_{op} corresponds to E_F instead of E_g, which corresponds to the well-known Burstein–Moss shift that is widely observed in degenerate narrow-gap semiconductors like HgCdTe.[29] As evident from Fig. 2, the deviation between E_{op} and E_g occurs at a temperature of $\sim$ 200 K, and increases with decreasing temperature. For example, at 11 K, E_{op} was measured to be 0.163 eV, which is 24% larger than the calculated E_g of 0.131 eV.

Generally, the position of the Fermi level in degenerate semiconductors can be calculated based on a free electron gas approximation combined with the Kane model in terms of band parameters such as E_g and P (conduction band-valence-band momentum matrix element).[32] By following the method

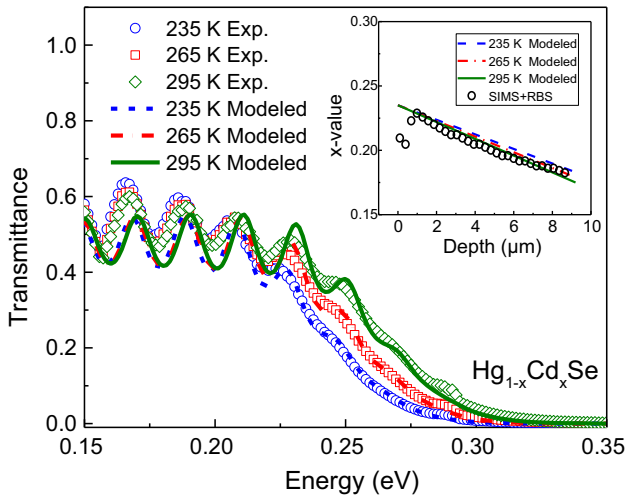

Fig. 4. Experimental (dots) and modeled (dashed or solid lines) infrared transmission spectra at temperatures of 235 K, 265 K, and 295 K of the graded HgCdSe sample. The inset shows the extracted x profile and compares it directly with the experimental x profile as obtained by SIMS combined with RBS.

reported in previous work on HgCdTe,[29] E_F can be calculated using a P value of 8.0×10^{-8} eV/cm.[5] As shown in Fig. 2, the calculated E_F for the sample with $n_B = 3.5 \times 10^{16}$ cm^{-3} agrees well with the observed E_{op} for $T < 200$ K, confirming the existence of the Moss–Burstein effect in our HgCdSe sample. With increasing temperature, the E_F moves closer to E_C, and eventually lies below E_C when $T > 200$ K. In this case, the sample becomes nondegenerate, and the vacant states are thermally distributed over an appreciable energy range ($\sim 4kT$) around E_F. As a consequence, optical absorption near E_g occurs, and E_{op} corresponds to E_g, as shown in Fig. 2. To meet the requirements of fabricating high-performance infrared detectors, further studies on annealing processes are needed to reduce the background doping level from 10^{16} to $< 10^{15}$ cm^{-3}. For a lower doping level of $n_B = 5.0 \times 10^{15}$ cm^{-3}, as indicated in Fig. 2, the deviation between E_g and E_{op} decreases from 20 meV to 0 meV at 77 K, confirming that the magnitude of the Burstein–Moss shift is highly dependent on doping level.

Traditional FTIR transmission spectral analysis has been widely used for determining the cut-off wavelength and thickness of IR thin film materials. However, the accuracy of the analysis is severely limited for detector structures with thin absorbers or with multi-layer two-color structures. For example, Doyle[2] utilized the 50% cut-off wavelength (and therefore the energy bandgap E_g) to deduce the x-value of MBE-grown $Hg_{1-x}Cd_xSe$ thin films according to the relationship between the bandgap at room temperature and the x value.[5] However, for samples with lower x-values (and thus narrower bandgaps) or with smaller thicknesses (and thus broader transmission edges), the transition cut-off is less

distinct, and thus this method becomes less reliable. In our experiments, the 50% cut-off energy at 310 K of the transmission spectrum is 0.266 eV, which is ~ 19 meV lower than the calculated E_g (0.285 eV) based on the nominal x-value. This suggests that the material composition (x-value) may not be uniform with depth, which thereby modifies the transition edge of the transmission spectrum. However, the E_{op} at 310 K deduced from the absorption spectrum (see Fig. 1b) is 0.282 eV, which is very close to the calculated value of E_g. Note that both of these two methods can only determine the average layer composition, and cannot provide information on the composition profile in a thin film.

In order to accurately characterize the thickness and composition in multi-layered HgCdTe, Sewell et al.[34] proposed a mathematical model for simulating the IR transmission spectra based on the characteristic matrix approach [36] in which the empirical formulae for calculating the absorption coefficients of HgCdTe are applied.[31] For the relatively less studied HgCdSe there are no empirical formulae available for calculating the absorption coefficients, so a similar approach to that used by Chu for HgCdTe [31] has been adopted using the reported transmission spectra of Bridgeman-grown $Hg_{1-x}Cd_xSe$ samples.[5] These bulk HgCdSe samples cover a wide range of x values ($0.15 < x < 0.3$, MWIR to VLWIR), and the absence of optical interference effects in the experimental absorption data renders them suitable for the data fitting process described later.

Figure 3a shows the RT experimental absorption spectra of Bridgeman-grown $Hg_{1-x}Cd_xSe$ samples with x varying from 0.15 to 0.3.[5] As evident from Fig. 3a, the spectra include a sharp absorption edge and a relatively flat region, except for the sample with x = 0.194 where only the absorption edge can be observed because of its relatively large thickness of 104 μm. Figure 3b shows the absorption spectra of the Bridgeman sample with x = 0.253 and a thickness of 14 μm measured at temperatures from 10 to 300 K. Theoretically, the intrinsic region ($E > E_g$) of the absorption spectra resulting from band to band transitions can be analyzed by using the optical transition theory and Kane model as undertaken by Summers for $Hg_{1-x}Cd_xSe$ [5] which, however, is a very complex procedure. As proposed by Chu in 1994,[31] an empirical formula for calculating the intrinsic optical absorption coefficient in the Kane region has been derived experimentally as follows:

$$\alpha = \alpha_g \exp\left[\beta(E - E_g)\right]^{1/2}, \tag{4}$$

where α_g is the intrinsic absorption coefficient at the bandgap E_g, and β is a parameter that depends on x value and temperature T. In addition, as confirmed in many materials, the absorption edge below the bandgap ($E < E_g$) follows Urbach's rule:

$$\alpha = \alpha_0 \exp\left[\frac{\delta(E - E_0)}{kT}\right], \tag{5}$$

where δ is a parameter that depends on x value and temperature T, and k is the Boltzmann constant, and the parameters α_0 and E_0 are constants that do not depend on photon energy E or temperature T. Thus, the absorption edges measured at different temperatures should converge to the same point, i.e. (E_0, α_0), while α_g and E_g can be obtained from the turning point where the sharp Urbach's tail ends and the plateau intrinsic region begins. The continuous condition for the two regions is δ/kT = (ln α_g-ln α_{g0})/($E_g - E_0$). The above parameters were adjusted to fit the experimental absorption data as follows:

$$\ln \alpha_0 = -21.03 + 52.27x \tag{6}$$

$$E_0 = -0.307 + 1.909x \tag{7}$$

$$\alpha_g = (-46.14 + 735.94x)\exp(0.0058T) \tag{8}$$

$$\beta = 185.82 + 0.227T + (150.9 - 3.205T)x \tag{9}$$

For the samples shown in Fig. 3, α_g increases slightly with increasing temperature and x value. It should be noted that the absorption coefficient model is valid for the case of non-degenerate conditions, since the Burstein-Moss effect is not considered. The solid lines shown in Fig. 3a and b represent the fitted results which generally agree well with the experimental spectra. As shown in Fig. 3b, some deviations between the experimental and calculated absorption spectra for the sample with x = 0.253 are observed for temperatures below 150 K, which is caused by the Burstein–Moss effect.

As demonstrated in Fig. 4, by employing the empirical expressions the non-degenerate infrared IR transmission spectra at 235 K, 265 K, and 295 K are able to be modeled. In the model, the 8.7 μm graded HgCdSe layer is treated as a sufficiently large stack of thin sub-layers, each with a constant local composition. The simulated transmittance edge is found to be very sensitive to the x value profile along the growth direction. Therefore, by adjusting the x profile along the growth direction to fit the experimental transmission edge at each temperature, the x profile along the growth direction can be deduced, the results of which are shown in the inset of Fig. 4. As evident from the inset, the extracted x profile agrees well with the experimental x profile as obtained by SIMS depth profiling combined with RBS. This agreement not only validates the wide applicability of the absorption coefficient model of HgCdSe in this work, but also demonstrates that the modeling of the FTIR transmission spectra can be used to characterize the x-value/Cd content in $Hg_{1-x}Cd_xSe$ materials, and

provides a useful non-destructive procedure for evaluating the composition uniformity, which is of significant importance for fabricating large-area imaging FPAs. Also, as illustrated in Fig. 4, some deviations between the simulated spectra and the experimental spectra in the passband region are also observed, which may be related to other non-idealities, such as surface/interface roughness, incoherent reflections from the GaSb substrate, and/or the inaccurate value of the refractive index of HgCdSe. For a more reliable extraction of the structural parameters, further studies on both the refractive index dispersion and absorption coefficient model of HgCdSe are required.

SUMMARY AND CONCLUSIONS

In summary, this work presents a temperature dependent FTIR spectroscopy study on MBE-grown $Hg_{1-x}Cd_xSe$ thin films on GaSb (211) substrates. The Burstein–Moss shift is observed at low temperatures, where the optical bandgap energy E_{op} corresponds to the calculated E_F instead of the bandgap E_g. In addition, empirical formulae for calculating the absorption coefficient of $Hg_{1-x}Cd_xSe$ alloys ($0.15 < x < 0.30$) based on previously-published data have been derived and used to model the composition profile of x value (composition) by fitting the experimental transmission data. The results of this study provide a useful tool for calculating the absorption coefficient and modeling the transmission spectra of HgCdSe thin films, which indicates that infrared transmission spectroscopy can be developed into a general tool for evaluating the compositional uniformity of HgCdSe, especially along the growth direction. More importantly, this analysis approach can also be applied to other infrared materials, including HgCdTe materials.

ACKNOWLEDGMENTS

This work was supported by the Australian Research Council (FT130101708, DP170104562, and LE170100233), and a Research Collaboration Awards from the University of Western Australia. Facilities used in this work are supported by the WA node of the Australian National Fabrication Facility (ANFF).

REFERENCES

1. K. Doyle, C.H. Swartz, J.H. Dinan, T.H. Myers, G. Brill, Y.P. Chen, B.L. VanMil, and P. Wijewarnasuriya, *J. Vac. Sci. Technol.* 31, 03C124 (2013).
2. K. Doyle, *Development of HgCdSe for Third Generation Focal Plane Arrays using Molecular Beam Epitaxy*. Texas State University San Marcos United States, 2013.
3. G.N. Brill, Y.P. Chen, P.S. Wijewarnasuriya, and N.K. Dhar, *Phys. Status Solidi A* 209, 1423 (2012).
4. Y.P. Chen, G. Brill, D. Benson, P. Wijewarnasuriya, and N. Dhar, *Proc SPIE* 8155, 815511 (2011).
5. C.J. Summers and J.G. Broerman, *Phys. Rev. B* 21, 559 (1980).
6. A. Rogalski, *Prog. Quantum Electron.* 27, 59 (2003).
7. A. Rogalski, J. Antoszewski, and L. Faraone, *J. Appl. Phys.* 105, 091101 (2009).
8. W. Lei, J. Antoszewski, and L. Faraone, *Appl. Phys. Rev.* 2, 041303 (2015).
9. J.P. Zanatta, G. Badano, C. Ph Ballet, J. Largeron, J. Baylet, O. Gravrand, J. Rothman, P. Castelein, J.P. Chamonal, and A. Million, *J. Electron. Mater.* 35, 1231 (2006).
10. L. He, L. Chen, Y. Wu, X.L. Fu, Y.Z. Wang, J. Wu, M.F. Yu, J.R. Yang, R.J. Ding, and X.N. Hu, *J. Cryst. Growth* 301, 268 (2007).
11. M. Reddy, J.M. Peterson, T. Vang, J.A. Franklin, M.F. Vilela, K. Olsson, E.A. Patten, W.A. Radford, J.W. Bangs, and L. Melkonian, *J. Electron. Mater.* 40, 1706 (2011).
12. M. Carmody, A. Yulius, D. Edwall, D. Lee, E. Piquette, R. Jacobs, D. Benson, A. Stoltz, J. Markunas, and A. Almeida, *J. Electron. Mater.* 41, 2719 (2012).
13. J. Wenisch, D. Eich, H. Lutz, T. Schallenberg, R. Wollrab, and J. Ziegler, *J. Electron. Mater.* 41, 2828 (2012).
14. W. Lei, R.J. Gu, J. Antoszewski, J. Dell, and L. Faraone, *J. Electron. Mater.* 43, 2788 (2014).
15. W. Lei, R.J. Gu, J. Antoszewski, J. Dell, G. Neusser, M. Sieger, B. Mizaikoff, and L. Faraone, *J. Electron. Mater.* 44, 3180 (2015).
16. W. Lei, Y.L. Ren, I. Madni, and L. Faraone, *Infrared Phys. Technol.* 92, 96 (2018).
17. C. R. Whitsett, J. G. Broerman, and C. J. Summers, in Semiconductors and Semimetals (Elsevier, 1981), Vol. 16, pp. 53.
18. C. R. Whitsett, J. G. Broerman, and C. J. Summers, in Defects, (HgCd)Se, (HgCd)Te (1981), pp. 53.
19. G. Brill, Y. Chen, and P. Wijewarnasuriya, *Proc Spie* 8155, 815512 (2011).
20. G. Brill, Y. Chen, and P. Wijewarnasuriya, *J. Electron. Mater.* 40, 1679 (2011).
21. F. C. Peiris, M. V. Lewis, G. Brill, Kevin Doyle and T. H. Myers, *J. Electron. Mater.* 47, 5715 (2018).
22. I. Madni, G.A. Umana-Membreno, W. Lei, and L. Faraone, *J. Electron. Mater.* 47, 5691 (2018).
23. W. Lei, Y.L. Ren, I. Madni, G.A. Umana-Membreno, and L. Faraone, *Infrared Phys. Technol.* 92, 197 (2018).
24. F.C. Peiris, G. Brill, K. Doyle, B. VanMil, and T.H. Myers, *J. Electron. Mater.* 43, 3056 (2014).
25. Y. Lansari, J.W. Cook, and J.F. Schetzina, *J. Electron. Mater.* 22, 809 (1993).
26. J. Chu, S. Xu, and D. Tang, *Appl. Phys. Lett.* 43, 1064 (1983).
27. E. Burstein, *Phys. Rev.* 93, 632 (1954).
28. T. S. Moss, In *Proc. Phys. Soc. London, Sect. B* 67, 775 (1954).
29. J. Chu, S. Xu, and D. Tang, *Phys. Scr.* 1986, 37 (1986).
30. M. Daraselia, M. Carmody, D.D. Edwall, and T.E. Tiwald, *J. Electron. Mater.* 34, 762 (2005).
31. J.H. Chu, B. Li, K. Liu, and D.Y. Tang, *J. Appl. Phys.* 75, 1234 (1994).
32. E.O. Kane, *J. Phys. Chem. Solids* 1, 249 (1957).
33. J.R. Lindle, W.W. Bewley, I. Vurgaftman, J.R. Meyer, J.L. Johnson, M.L. Thomas, and W.E. Tennant, *Phys. E* 20, 558 (2004).
34. R.H. Sewell, J.M. Dell, C.A. Musca, and L. Faraone, *Microelectronics: Design Technology, and Packaging* 5274, 215 (2004).
35. F. Urbach, *Phys. Rev.* 92, 1324 (1953).
36. D.E. Aspnes, *Thin Solid Films* 89, 249 (1982).